Superconducting properties of the noncentrosymmetric superconductor Re_6Hf

D. Singh,[1] A. D. Hillier,[2] A. Thamizhavel,[3] and R. P. Singh[1,*]

[1]*Indian Institute of Science Education and Research Bhopal, Bhopal 462066, India*

[2]*ISIS facility, STFC Rutherford Appleton Laboratory, Harwell Science and Innovation Campus, Oxfordshire, OX11 0QX, United Kingdom*

[3]*Department of Condensed Matter Physics and Materials Science, Tata Institute of Fundamental Research, Mumbai 400005, India*

(Received 12 May 2016; revised manuscript received 19 July 2016; published 22 August 2016)

We report synthesis and detailed characterization of the noncentrosymmetric superconductor Re_6Hf using powder x-ray diffraction (XRD), magnetization, transport, and thermodynamic measurements. XRD confirmed the noncentrosymmetric, α-*Mn* cubic structure in Re_6Hf with the cubic cell parameter $a = 9.6850(3)$ Å. Resistivity, DC, and AC magnetization measurements confirmed the type-II superconductivity in Re_6Hf with the transition temperature $T_c^{\text{onset}} \sim 5.96$ K, having the lower critical field $H_{c1}(0)$ 5.6 mT and upper critical field $H_{c2}(0)$ 12.2 T. The electronic specific heat data fits well with the single-gap BCS model. The Sommerfeld coefficient (γ) also shows linear relation with the magnetic field. All above results suggest *s*-wave superconductivity in Re_6Hf.

DOI: 10.1103/PhysRevB.94.054515

I. INTRODUCTION

In 1957, Bardeen, Cooper, and Schrieffer (BCS) explained the origin of superconductivity using the concept of Cooper pairs [1]. Cooper pairs are formed from electrons that have equal and opposite crystal momenta and spin. Since electrons are fermions, the wave function must be antisymmetric with respect to the exchange of two electrons. The two electron wave function can be made asymmetric by considering the spatial and spin components. If the spatial wave function is symmetric/antisymmetric, then the spin wave function must be antisymmetric/symmetric. This is termed as spin-singlet state/spin-triplet state. This scenario is only possible if inversion symmetry is present in crystal structure [2,3].

There have been intense theoretical and experimental studies on superconducting systems lacking spatial inversion symmetry, following the discovery of unconventional superconductivity in the noncentrosymmetric (NSC) heavy fermion compound $CePt_3Si$ [4]. In a NCS superconductor (SC), the absence of the center of inversion induces Rashba-type antisymmetric spin-orbit coupling (ASOC) due to an asymmetric potential gradient along the crystal axis. This momentum dependent spin structure in consequence lifts the degeneracy of the conduction band electrons at the Fermi surface resulting into the possible mixing of spin-singlet and spin-triplet pairing states. The magnitude of ASOC splitting actually dictates the extent of mixing of spin-singlet and spin-triplet components [5–10]. The possible mixing of pair states in NCS superconductors may lead to various superconducting properties such as the upper critical field exceeding Pauli limit, point or line nodes in the superconducting gap parameter resulting into nodal excitations in penetration depth, heat capacity and other thermodynamic measurements, and time reversal symmetry breaking in the superconducting condensate [11].

Apart from $CePt_3Si$ several other Ce- and U-based heavy fermionic NCS SCs, e.g., $CeRhSi_3$ [12,13], $CeIrSi_3$ [14,15], $CeCoGe_3$ [16], and UIr [17] were discovered with applied pressure, however this does not resolve the problem as strong electron correlations in the *f*-electron systems with superconductivity at the vicinity of the magnetic quantum critical point hinder the pursuit to realize the effects of ASOC and the absence of an inversion center on superconductivity. Superconductivity in these systems is expected to be due to the unconventional pairing mechanism, most likely driven by magnetic fluctuations. Hence, several weakly correlated and nonmagnetic NCS superconducting systems, e.g., $Li_2(Pd,Pt)_3B$ [18–22], $LaNiC_2$ [23,24], Y_2C_3 [25], L_2C_3 [26] Re_3W [27], $Mg_{10}Ir_{19}B_{16}$ [28], La*MP*(*M*=Ir, Rh and *P*=P, As) [29], Mo_3Al_2C [30,31], Rh_2Ga_9 [32,33], Ir_2Ga_9 [32,33], Ru_7B_3 [34–36], $Nb_{0.18}Re_{0.82}$ [37–39], La_7Ir_3 [40], and Re_6Zr [41,42] were investigated to understand the primary mechanism for unconventional superconductivity in NCS SCs. It was found that only a few of them exhibited unconventional superconducting behavior including triplet pairing [10,22,40,41,43] and upper critical field close to the Pauli limit [25,31]. Others exhibited only dominant *s*-wave character.

Theoretical results suggest that ASOC play an important role in controlling the mixing of spin-singlet and spin-triplet pairing channel. In NCS superconductor $Li_2(Pd,Pt)_3B$ [10,18–22,44], it was shown that the pairing state can be tuned from spin-singlet to spin-triplet by changing the strength of ASOC. Here substitution of the Pt element with strong spin-orbital coupling to the site of the Pd element changes the overall mixing of pairing states leading to unconventional superconductivity.

Recently, noncentrosymmetric superconductor Re_6Zr shows an unconventional superconducting ground state having the signature of time reversal symmetry breaking with dominant *s*-wave pairing by muon spectroscopy [41]. As spin-orbital coupling varies as Z^4, by substituting Zr by Hf, the strength of the spin-orbit coupling can be enhanced by a factor of 10 in Re_6Hf compared to Re_6Zr. This in turn may increase the contribution of the spin-triplet component in the superconducting ground state. In this paper, we present the results of measured superconducting properties of intermetallic binary compound Re_6Hf exhibiting bulk superconductivity at $T_c^{\text{onset}} \sim 5.96$ K. Superconducting properties were determined by resistivity, magnetization, and specific heat measurements in Re_6Hf and results were compared to Re_6Zr to elucidate the effects of enhanced ASOC.

*rpsingh@iiserb.ac.in

II. EXPERIMENTAL DETAILS

A polycrystalline sample of Re_6Hf (3g) was synthesized using the standard arc-melting technique where the stoichiometric amounts of Hf(4N) and Re(4N) were taken in a nominal ratio of 6:1 on a water cooled copper hearth under the flow of high purity argon gas. Both the elements were melted together to make a single button of Re_6Hf, then flipped and remelted several times for the sample homogeneity. The sample formed was hard and silvery gray in color with negligible mass loss.

X-ray diffraction (XRD) was carried out on a PANalytical diffractometer equipped with CuK_α radiation ($\lambda = 1.54056$ Å) for the characterization of crystal structure and phase purity. Magnetization and AC susceptibility measurements were performed using a Quantum Design superconducting quantum interference device (MPMS 3, Quantum Design). In magnetization measurement, the sample was cooled down to 1.8 K in zero field and then a field of 10 mT was applied. The data were recorded while warming it to 10 K called ZFCW mode, whereas in the FCC mode, the sample was cooled down to 1.8 K in a 10 mT field with data taken simultaneously. Magnetization and AC susceptibility measurements were also done under different applied fields in a temperature range of 1.8 K to 8.0 K in magnetic fields up to 7.0 T. Specific heat measurements were performed by the two tau time-relaxation method using the physical property measurement system (PPMS, Quantum Design, Inc.) in zero field and under applied magnetic fields up to 7.0 T. The electrical resistivity measurement was performed on the PPMS by using a conventional four-probe ac technique at frequency 157 Hz and excitation current 10 mA. The measurement was done in zero field from 1.85 K to 300 K to know the residual resistivity ρ_0 and residual resistivity ratio (RRR).

III. RESULTS AND DISCUSSION

A. Sample characterization

Polycrystalline sample of Re_6Hf was crushed into a very fine powder for XRD analysis. The powder XRD data was collected at room temperature as shown in Fig. 1. Rietveld refinement was performed using High Score Plus Software. The refinement shows that the sample is in single phase with no impurity. Re_6Hf crystallizes into a cubic, noncentrosymmetric *α-Mn* structure with lattice cell parameter $a = 9.6850(3)$ Å. The primitive Bravais lattice adopts the space group $I\bar{4}3m$ (space group no. 217). There are around eight formula units per unit cell. The material is intrinsically disordered, which is reflected in the low value of the residual resistivity ratio and high residual resistivity seen in the section below. Refined cell parameters and atomic positions are shown in Table I.

B. Normal and superconducting state properties

1. *Electrical resistivity*

The temperature dependence of the resistivity for Re_6Hf between 1.85 K and 300 K in zero magnetic field is shown in Fig. 2(a). Resistivity increases leisurely with temperature showing poor metallic behavior. The residual resistivity ratio is found to be $\rho(300)/\rho(10) = 1.47$, which is very small, suggesting that resistivity has either little temperature dependence

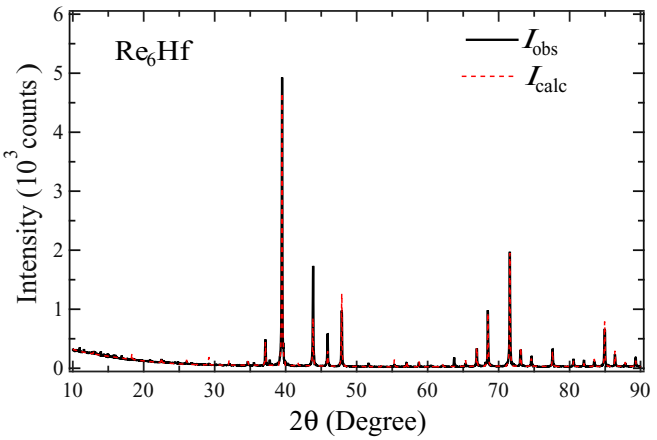

FIG. 1. Powder XRD pattern for the Re_6Hf sample recorded at room temperature using CuK_α radiation. Rietveld refined calculated pattern for cubic noncentrosymmetric *α-Mn* (217) structure is shown by a dotted red line.

or is dominated by disorder. This behavior is similar to other Re based *α-Mn* compounds $Nb_{0.18}Re_{0.82}$ (RRR ∼ 1.3) [37], $Re_{24}Ti_5$ (RRR ∼ 1.3) [45], and Re_6Zr (RRR ∼ 1.10) [41,42]. An expanded plot of the zero-field resistivity data ρ(T) is shown in the inset of Fig. 2(a), which shows a superconducting transition at the onset temperature $T_c^{\text{onset}} = 5.96$ K, with the transition width of $\Delta T = 0.41$ K.

The low temperature resistivity data have been fitted to a power law

$$\rho = \rho_0 + AT^2 \tag{1}$$

from 10 K $\leqslant T \leqslant$ 50 K, as shown in Fig. 2(b) by the solid red line. First term ρ_0 is the residual resistivity due to crystallographic defects and the second term is the electronic contribution to resistivity due to electron-electron scattering at low temperatures in the Fermi-liquid picture. Here A is taken as a measure of the degree of electron-electron correlation.

By fitting Eq. (1), we obtained $\rho_0 = 106.12 \pm 0.02$ $\mu\Omega$ cm and $A = (2.79 \pm 0.01) \times 10^{-3}$ $\mu\Omega$ cm K^{-2}. The higher value of ρ_0 is most likely due to the polycrystalline nature of the sample. The value of A is low, indicating a weakly correlated system. Resistivity doesn't increase significantly

TABLE I. Crystal structure parameters obtained from the Rietveld refinement of the room temperature powder x-ray diffraction of Re_6Hf.

Structure	Cubic
Space group	$I\bar{4}3m$
Lattice parameters	
a (Å)	9.6850(3)
V_{cell} (Å^3)	908

Atomic Coordinates

Atom	Wyckoff position	x	y	z
Re1	24g	0.106	0.106	0.288
Re2	24g	0.344	0.344	0.031
Hf1	8c	0.315	0.315	0.315
Hf2	2a	0	0	0

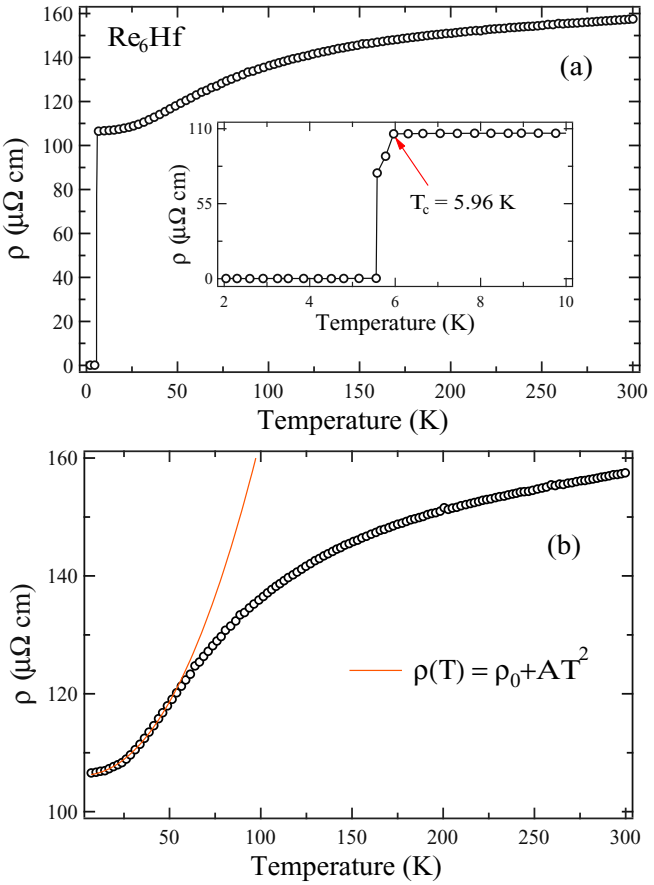

FIG. 2. (a) Temperature dependence of the resistivity for Re_6Hf shown over the range 1.85 K $\leqslant T \leqslant$ 300 K. The inset shows the superconducting transition at $T_c^{\text{onset}} = 5.96$ K. (b) Quadratic temperature dependence over the temperature range 10 K $\leqslant T \leqslant$ 50 K indicating Fermi-liquid behavior at low temperature.

from its residual resistivity ρ_0 value in the fitted temperature range due to dominance by disorder but shows a quadratic temperature dependence as shown in Fig. 2(b), which can be described by Fermi-liquid behavior [31,37,42,45,46].

2. *Magnetization*

The superconductivity in Re_6Hf was confirmed by the magnetization data taken in ZFCW and FCC mode as shown in Fig. 3. The data were taken in low applied field of 10 mT, showing the onset of strong diamagnetic signal due to superconducting transition at $T_c^{\text{onset}} = 5.94$ K. Superconducting transition was further confirmed by AC susceptibility (Fig. 4) measurement.

Figure 5(a) shows the low field (0–30 mT) magnetization curves $M(H)$ for Re_6Hf taken at different temperatures. Lower critical field H_{c1}(T) is defined as the field deviating from the linear line for initial slope in magnetization curve. The H_{c1} is 5.2 mT at $T = 1.8$ K and decreases monotonically with increase in temperature to 1.0 mT at $T = 5.5$ K. The temperature variation of H_{c1}(T) is shown in Fig. 5(b). As expected H_{c1}(T) varies as a function of T^2 in accordance with

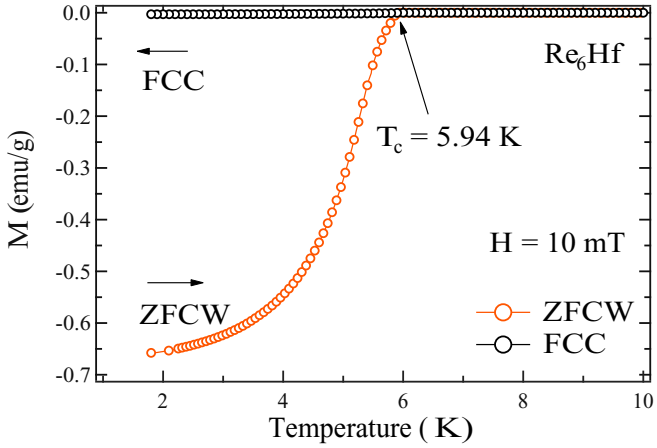

FIG. 3. Temperature dependence of the magnetic moment, collected via zero-field cooled warming (ZFCW) and field cooled cooling (FCC) methods under an applied field of 10 mT.

Ginzburg-Landau (GL) theory

$$H_{c1}(T) = H_{c1}(0)\left(1 - \left(\frac{T}{T_c}\right)^2\right). \tag{2}$$

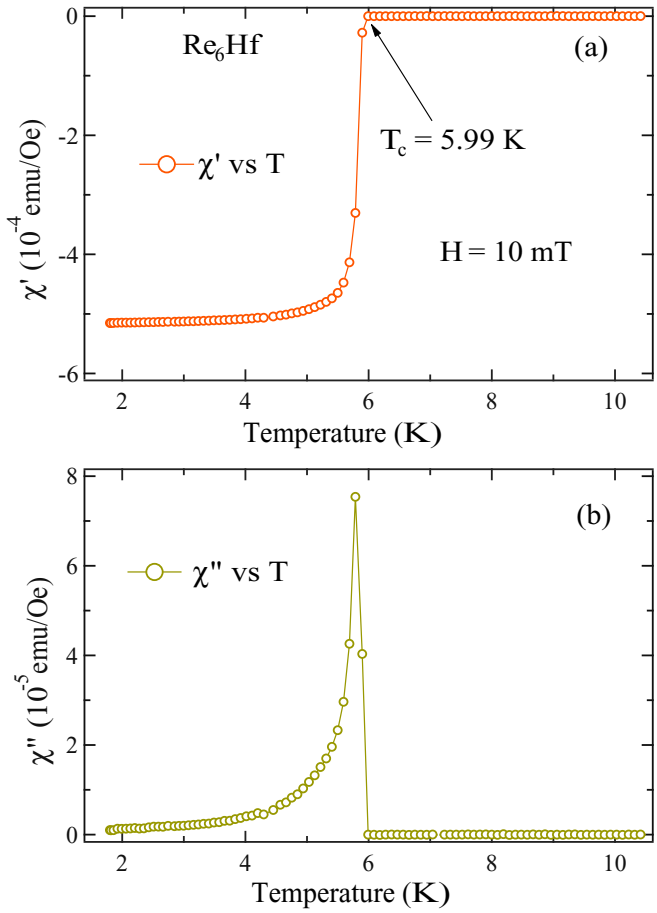

FIG. 4. Temperature dependence of [(a) real and (b) imaginary] AC susceptibility for Re_6Hf.

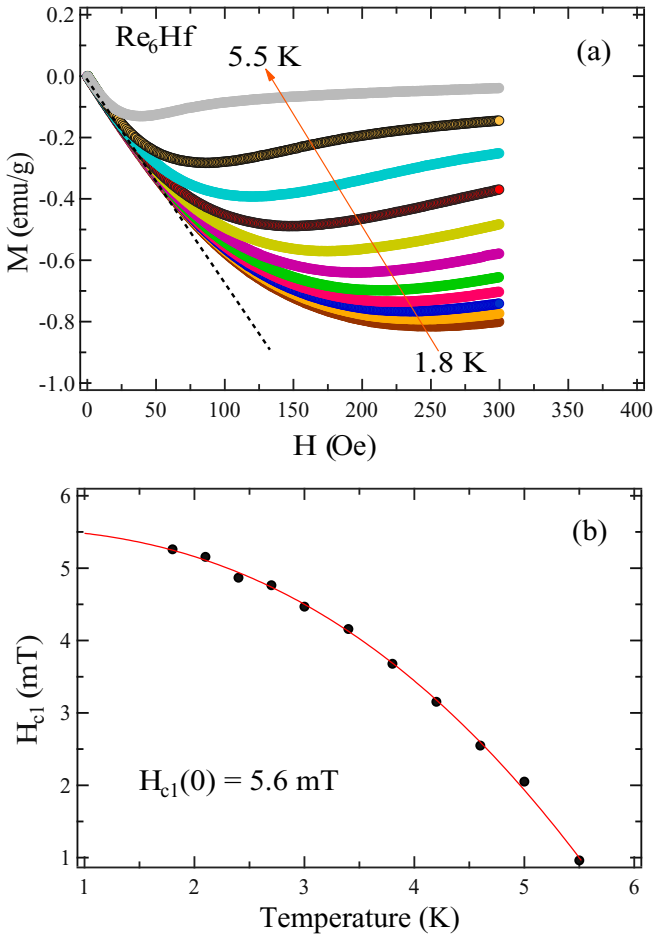

FIG. 5. (a) Low-field magnetization curves for Re_6Hf at various temperatures (b) Temperature dependence of the lower critical field H_{c1} was fitted using Ginzburg-Landau relation gives $H_{c1}(0) \sim 5.6$ mT.

Lower critical field $H_{c1}(0)$ was estimated to be 5.6 ± 0.5 mT by fitting the relation given in Eq. (2) in the data given in Fig. 5(b).

A magnetization curve at 1.8 K in high applied magnetic field range (± 7 T) is shown in Fig. 6. As evident from the graph, Re_6Hf exhibits a conventional type-II superconductivity. H_{Irr} estimated from magnetization curve is 1.80 T at 1.8 K, here for fields $H > H_{Irr}$ unpinning of vortices starts taking place.

3. *Specific heat*

Specific heat $C(T)$ measurement for Re_6Hf in zero field in the temperature range 1.85 K $\leqslant T \leqslant$ 10 K is shown in Fig. 7(a). The superconducting transition in specific heat data is manifested by a sharp jump in $C(T)$ at $T_c = 5.96$ K, confirming bulk superconductivity in Re_6Hf. The field dependence of the specific heat is shown in Fig. 7(b), where a jump near T_c moves to lower temperature and the size of the jump ΔC becomes smaller with increasing magnetic field. The low temperature normal state specific heat can be extracted easily with the relation

$$\frac{C}{T} = \gamma_n + \beta_3 T^2 + \beta_5 T^4, \qquad (3)$$

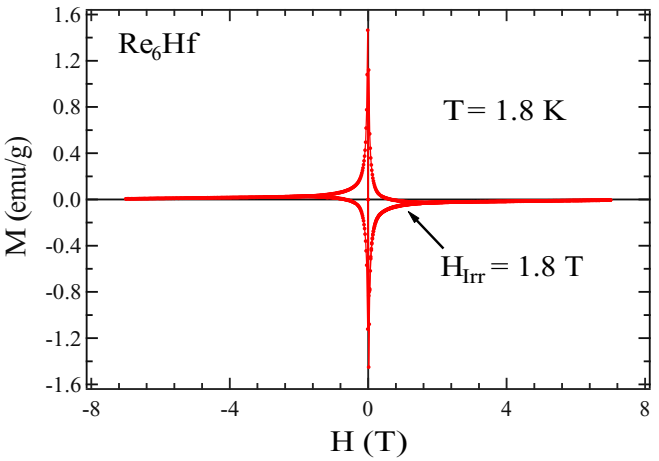

FIG. 6. Magnetization vs magnetic field variation at $T = 1.8$ K. The magnetization is irreversible below a field $H_{Irr} = 1.8$ T.

where the extrapolation of normal state behavior below T_c, to the $T \to 0$ limit, allows the determination of normal state Sommerfeld coefficient γ_n, Debye constant β_3, and the anharmonic contribution β_5 to the specific heat. By fitting Eq. (3) between 36 K $\leqslant T^2 \leqslant$ 100 K, as shown by the solid

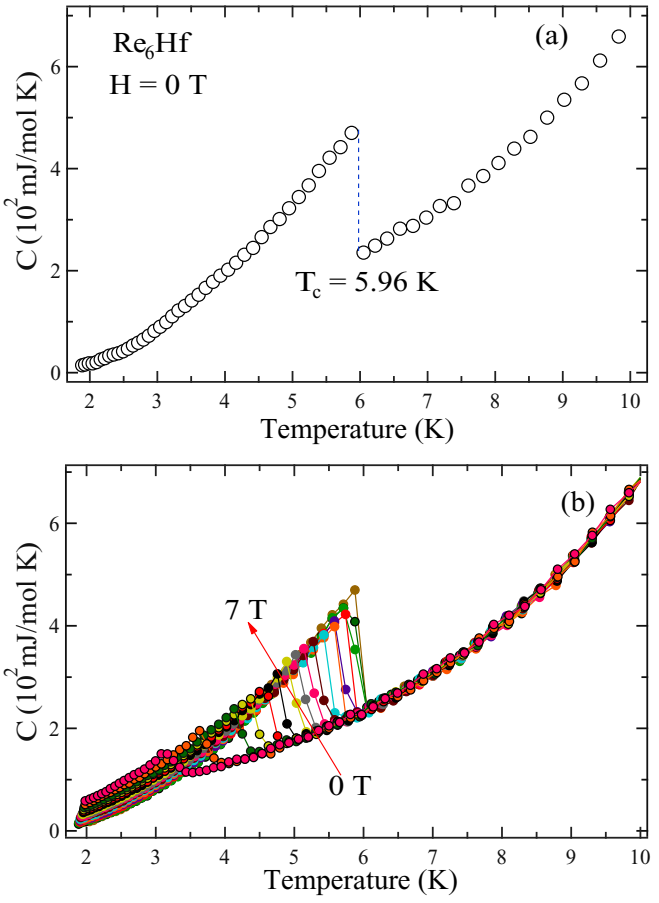

FIG. 7. (a) Temperature dependence of specific heat in zero field showing superconducting transition at $T_c = 5.96$ K. (b) Field dependence of the specific heat data, showing the suppression of T_c with increasing field.

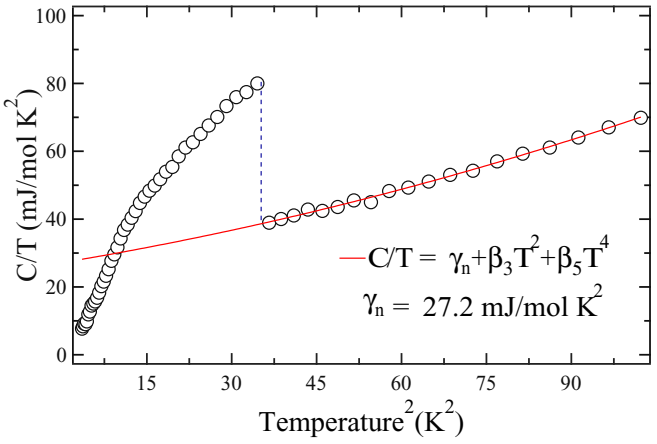

FIG. 8. C/T vs T^2 for 36 K $\leqslant T^2 \leqslant$ 100 K in zero field well described by the equation $\frac{C}{T} = \gamma_n + \beta_3 T^2 + \beta_5 T^4$.

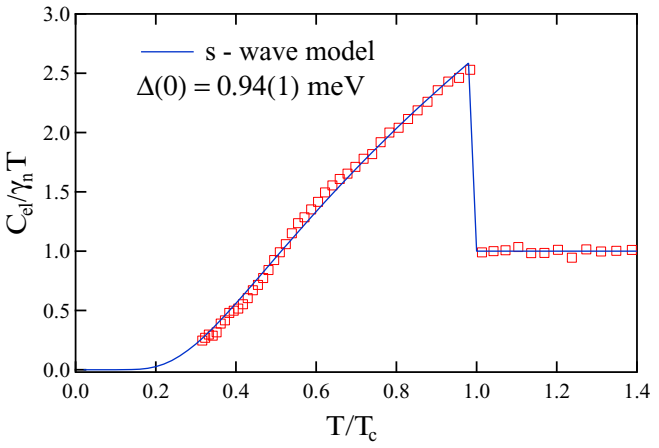

FIG. 9. Solid green curve in $C_{el}/\gamma_n T$ versus T/T_c data show the single-gap BCS model fitting for $\alpha = \Delta(0)/k_B T_c = 1.82$.

red line in Fig. 8, we obtained $\gamma_n = 27.2 \pm 0.1$ mJ mol^{-1} K^{-2}, $\beta_3 = 0.28 \pm 0.05$ mJ mol^{-1} K^{-4}, and $\beta_5 = 0.0014 \pm 0.0003$ μJ mol^{-1} K^{-6}.

The Debye temperature θ_D is related to the β_3 coefficient through the formula

$$\theta_D = \left(\frac{12\pi^4 RN}{5\beta}\right)^{\frac{1}{3}} \tag{4}$$

where R is the molar gas constant (=8.314 J mol^{-1} K^{-1}). Using N (=7) the number of atoms per formula unit, it gives $\theta_D = 364$ K. For noninteracting particles, the Sommerfeld coefficient is proportional to the density of states $D_C(E_F)$ at the Fermi level which is calculated to be 11.53 $\frac{\text{states}}{eVf.u}$ from the relation given by

$$\gamma_n = \left(\frac{\pi^2 k_B^2}{3}\right) D_C(E_f) \tag{5}$$

where $k_B \approx 1.38 \times 10^{-23}$ J K^{-1}.

This calculated density of states $D_C(E_f)$, and the effective mass m^* of quasiparticles, contains the influence of the many body electron-phonon interaction and is related to the bare band-structure density of states $D_{\text{band}}(E_f)$ and m^*_{band} according to relation

$$D_C(E_f) = D_{\text{band}}(E_f)(1 + \lambda_{e\text{-}ph}) \tag{6}$$

$$m^* = m^*_{\text{band}}(1 + \lambda_{e\text{-}ph}) \tag{7}$$

where $\lambda_{e\text{-}ph}$ is the dimensionless electron-phonon coupling constant. The electron-phonon coupling constant which gives the strength of attractive interaction between electron and phonon can be calculated using θ_D and T_c given in McMillan theory [47] by

$$\lambda_{e-ph} = \frac{1.04 + \mu^* ln(\theta_D/1.45T_c)}{(1 - 0.62\mu^*) ln(\theta_D/1.45T_c) - 1.04} \tag{8}$$

where μ^* is the repulsive screened coulomb parameter, typically given by $\mu^* = 0.13$ for many intermetallic superconductors. Using $T_c = 5.96$ K (from our specific heat measurement) we obtained $\lambda_{e\text{-}ph} = 0.63$. This value is comparable to other fully gapped noncentrosymmetric superconductors such as 0.6 for $Re_{24}Ti_5$ [45], 0.5 for $Nb_{0.18}Re_{0.82}$ [37], Re_6Zr [42], and $SrAuSi_3$ [48] suggesting that Re_6Hf is a moderately coupled superconductor. Using the value of $\lambda_{e\text{-}ph}$, we calculated $D_{\text{band}}(E_f)$ equal to 7.04 $\frac{\text{states}}{eVf.u}$. Also by taking $m^*_{\text{band}} = m_e$ the effective mass for the quasiparticles comes out to be 1.63 m_e.

The electronic contribution to the specific heat in the superconducting state $C_{el}(T)$ can be calculated by subtracting the phononic contribution from the measured data $C(T)$

$$C_{el}(T) = C(T) - \beta_3 T^3 + \beta_5 T^5. \tag{9}$$

The magnitude of the specific heat jump $\frac{\Delta C_{el}}{T_c}$ at T_c is 41.55 mJ mol^{-1} K^{-2}. This gives the normalized specific heat jump $\frac{\Delta C_{el}}{\gamma_n T_c} = 1.53$ for $\gamma_n = 27.2$ mJ mol^{-1} K^{-2}, which is slightly higher than the BCS value of $\frac{\Delta C_{el}}{\gamma_n T_c} = 1.43$ in the weak coupling limit.

The temperature dependence of the specific heat data in the superconducting state can best be described by the single-gap BCS expression for normalized entropy S

$$\frac{S}{\gamma_n T_c} = -\frac{6}{\pi^2}\left(\frac{\Delta(0)}{k_B T_c}\right)\int_0^\infty [f \ln(f) + (1-f)\ln(1-f)]dy \tag{10}$$

where $f(\xi) = [\exp(E(\xi)/k_B T)+1]^{-1}$ is the Fermi function, $E(\xi) = \sqrt{\xi^2 + \Delta^2(t)}$, where ξ is the energy of normal electrons measured relative to the Fermi energy, $y = \xi/\Delta(0)$, $t = T/T_c$, and $\Delta(t) = \tanh[1.82(1.018((1/t) - 1))^{0.51}]$ is the BCS approximation for the temperature dependence of the energy gap. The normalized electronic specific heat is related to the normalized entropy by

$$\frac{C_{el}}{\gamma_n T_c} = t\frac{d(S/\gamma_n T_c)}{dt} \tag{11}$$

where C_{el} below T_c is described by Eq. (11), whereas above T_c it is equal to $\gamma_n T_c$. Figure 9 shows the fitting of specific heat data to Eq. (11) which yields $\alpha = \Delta(0)/k_B T_c = 1.82 \pm 0.03$, which is slightly larger than the BCS value $\alpha_{BCS} = 1.764$ in the weak coupling limit, suggesting a moderately coupled superconductivity in Re_6Hf as concluded from the value of $\lambda_{e\text{-}ph}$ obtained earlier.

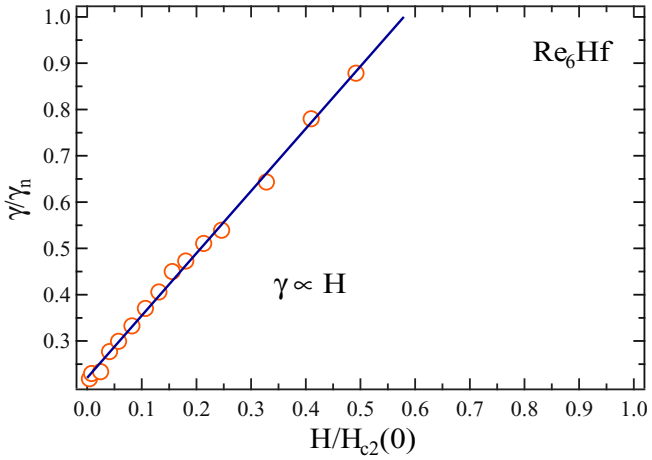

FIG. 10. γ and H were plotted versus each other after normalizing by $\gamma_n (= 27.2$ mJ mol^{-1} K$^{-2})$ and $H_{c2}(0) (= 12.2$ T). Solid blue curve in γ/γ_n versus $H/H_{c2}(0)$ plot show the linear relation indicating s-wave superconductivity in Re_6Hf.

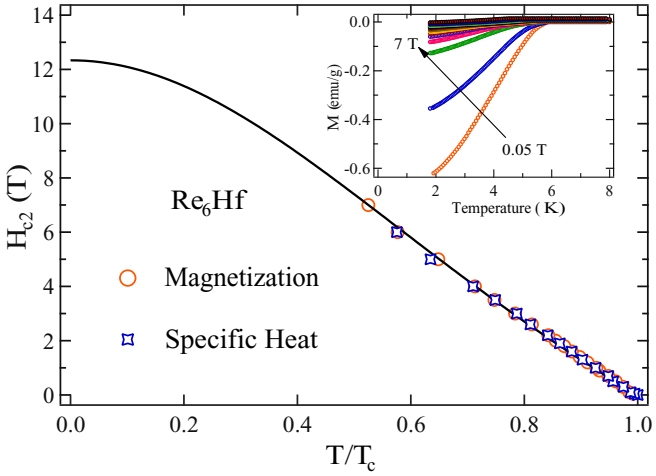

FIG. 11. Determination of the upper critical field $H_{c2}(0)$ via magnetization and heat capacity measurements. The solid lines are Ginzburg-Landau [Eq. (14)] fits. The inset shows the $M(T)$ curves for various applied magnetic fields.

In the α model BCS parameter α_{BCS} is replaced by α which can be determined from the jump ΔC_{el} at T_c according to the formula $\Delta C_{el}/\gamma_n T_c = 1.426(\alpha/\alpha_{BCS})^2$. Substituting the value of normalized specific heat jump $\Delta C_{el}/\gamma_n T_c = 1.53$ for our sample, we get $\alpha = 1.82$ which is in good agreement with the fitted value obtained above showing the consistency of the method.

The fully gapped s-wave superconductivity in Re_6Hf can also be confirmed by the magnetic field dependence of the Sommerfeld coefficient $\gamma(H)$. The Sommerfeld coefficient is proportional to the vortex density in a conventional fully gapped type-II superconductor. Therefore, as we apply more field the vortex density increases due to an increase in the number of field induced vortices which in turn enhances the quasiparticle density of states. This gives rise to a linear relation between γ and H, i.e., $\gamma(H) \propto H$ for a nodeless and isotropic s-wave superconductor [48–50]. For a superconductor with nodes in the gap, Volovik predicted a nonlinear relation given by $\gamma(H) \propto H^{\frac{1}{2}}$ [51].

The Sommerfeld coefficient γ was calculated by fitting Eq. (12) in C_{el}/T versus T data for various fields and extrapolating it to $T = 0$ K [48]

$$\frac{C_{el}}{T} = \gamma + \frac{A}{T}\exp\left(\frac{-bT_c}{T}\right). \tag{12}$$

Field dependence of γ is shown in Fig. 10 where we can clearly observe a linear relation between $\gamma(H)$ and H confirming the s-wave superconductivity in Re_6Hf which we have already seen by the single-gap BCS fitting in low temperature specific heat measurement.

The condensation energy U (0) can be calculated using γ and $\alpha (= \Delta(0)/k_B T_c)$ from the relation

$$U(0) = \frac{1}{2}\Delta^2(0) D_{\text{band}}(E_f) = \frac{3\gamma_n \Delta^2(0)}{4\pi^2 k_B^2} \tag{13}$$

which gives $U(0) = 246.1$ mJ mol^{-1}. The magnitude of electron-electron correlation can be given by Kadowaki-Woods ratio, which is given by $K_w = \frac{A}{\gamma_n^2}$, where A is the coefficient of the quadratic temperature dependent resistivity term, whereas γ_n is the normal state Sommerfeld coefficient. In heavy fermionic systems where electron-electron correlation is significant the Kadowaki-Woods ratio K_w approaches 1×10^{-5} $\mu\Omega$ cm mJ^{-2}mole^2 K^2 [52–54]. For $A = 0.00279$ $\mu\Omega$ cm K^{-2} and $\gamma_n = 27.2$ mJ mol^{-1} K^{-2}, we found $K_w = 0.37 \times 10^{-5}\mu\Omega$ cm mJ^{-2} mole^2 K^2 which is smaller than strongly correlated systems indicating that Re_6Hf is a weakly correlated system.

Isothermal magnetization measurement was done in magnetic fields up to 7.0 T to calculate the upper critical field $H_{c2}(0)$ as shown in the inset of Fig. 11. The transition temperature T_c was taken as the onset of the diamagnetic signal in magnetization measurement. As the field increases, T_c shifts to lower temperature with the superconducting transition becoming broader. H_{c2}(T) was seen to be varying linearly when plotted against reduced temperature (T/T_c) as displayed in Fig. 11, and can be fitted using the Ginzburg-Landau (GL) formula to calculate $H_{c2}(0)$

$$H_{c2}(T) = H_{c2}(0)\frac{(1-t^2)}{(1+t^2)} \tag{14}$$

where t $= T/T_c$. Our experimental data fits fairly well with Eq. (14) yielding the upper critical field $H_{c2}(0)$ to be around 12.2 ± 0.1 T. The similar linear behavior of H_{c2}(T) was noted when calculated from specific heat measurements $C(T)$ as shown by blue data points in Fig. 11; when fitted with GL formula it gives $H_{c2}(0) \approx 12.2$ T.

$H_{c2}(0)$ can be used to estimate the Ginzburg Landau coherence length ξ_{GL} from the relation [55]

$$H_{c2}(0) = \frac{\Phi_0}{2\pi\xi_{GL}^2} \tag{15}$$

where $\Phi_0 (= 2.07 \times 10^{-15}$ Tm$^2)$ is the magnetic flux quantum. Using $H_{c2}(0) = 12.2$ T we calculated $\xi_{GL}(0) \approx 52$ Å.

In a type-II superconductor, Cooper pair breaking due to the applied magnetic field is attributed to two types of mechanisms: orbital and Pauli paramagnetic limiting field

effect. In orbital pair breaking, the field-induced kinetic energy of a Cooper pair exceeds the superconducting condensation energy, whereas in Pauli paramagnetic limiting it is energetically favorable for the electron spins to align with the magnetic field, thus breaking the Cooper pairs. For BCS superconductors, the orbital limit of the upper critical field $H_{c2}^{\text{orbital}}(0)$ was given by the Werthamer-Helfand-Hohenberg (WHH) expression [56,57]

$$H_{c2}^{\text{orbital}}(0) = -\alpha T_c \frac{dH_{c2}(T)}{dT}\bigg|_{T=T_c} \tag{16}$$

where α is the purity factor given by 0.693 for dirty limit superconductors and 0.73 for clean limit superconductors. Initial slope $\frac{-dH_{c2}(T)}{dT}|_{T=T_c}$ calculated from the H_{c2}-T phase diagram is 2.36 T K^{-1}, which gives the orbital limiting upper critical field $H_{c2}^{\text{orbital}}(0) \approx 9.77$ T in the dirty limit. The Pauli limiting field within the BCS theory is given by $H_{c2}^{p}(0) = 1.86\ T_c$ [58,59], which for $T_c = 5.96$ K gives $H_{c2}^{p}(0) \approx 11.10$ T. The Maki parameter [60] α_M is the measure of relative strengths of the orbital and Pauli limiting values of H_{c2} and is given by

$$\alpha_M = \sqrt{2} H_{c2}^{orb}(0)/H_{c2}^{p}(0). \tag{17}$$

From this relation we obtain $\alpha_M = 1.24$. The sizable value of Maki parameter obtained from this expression is an indication that the effect of Pauli limiting field is non-negligible [37]. Since upper critical field $H_{c2}(0)$ calculated above is close to both the orbital limiting field and Pauli limiting field, it is highly desirable to do the detailed investigations of the upper critical field in high quality single crystals of Re_6Hf. If $H_{c2}(0)$ actually exceeds Pauli limit in clean single crystals of Re_6Hf, it confirms the contribution of spin-triplet component in superconducting pairing state. Anisotropic measurements of upper critical field $H_{c2}(0)$ also aspires since the paramagnetic pair breaking effect depends on the spin structure of the paired electrons in momentum space which can give more information on effects of the ASOC and broken inversion symmetry on the superconducting state.

The Ginzburg Landau penetration depth $\lambda_{GL}(0)$ can be obtained from $H_{c1}(0)$ and $\xi_{GL}(0)$ using the relation [28]

$$H_{c1}(0) = \left(\frac{\Phi_0}{4\pi\lambda_{GL}^2(0)}\right) ln\left(\frac{\lambda_{GL}(0)}{\xi_{GL}(0)}\right). \tag{18}$$

For $H_{c1}(0) \approx 5.6$ mT and $\xi_{GL}(0) = 52$ Å, we obtained $\lambda_{GL}(0) \approx 3538$ Å.

The Ginzburg Landau (GL) parameter is given by the relation

$$k_{GL} = \frac{\lambda_{GL}(0)}{\xi_{GL}(0)}. \tag{19}$$

For $\xi_{GL}(0) = 52$ Å and $\lambda_{GL}(0) = 3538$ Å, we get $k_{GL} \approx 68$. GL parameter $k_{GL} \gg \frac{1}{\sqrt{2}}$, indicating that Re_6Hf is a strong type-II superconductor. Thermodynamic critical field H_c is obtained from k_{GL}, $H_{c1}(0)$, and $H_{c2}(0)$ using the relation [28]

$$H_{c1}(0)H_{c2}(0) = H_c^2 ln k_{GL} \tag{20}$$

yielding H_c around 126.7 mT.

Ginzburg number G_i is the ratio of thermal energy k_BT (where the upper limit of T is T_c) to condensation energy associated with coherence volume, which measures the sensitivity of the vortex system against thermal fluctuations [61,62]

$$G_i = \frac{1}{2}\left(\frac{k_B\mu_0\tau T_c}{4\pi\xi^3(0)H_c^2(0)}\right)^2 \tag{21}$$

where τ is the anisotropy parameter which is 1 for cubic Re_6Hf. For $\xi_0 = 52$ Å, $H_c(0) = 126.7$ mT, and $T_c = 5.96$ K, we got $G_i = 6.65 \times 10^{-2}$. It was already noticed from the magnetization curve that melting of vortices starts at field $H > H_{Irr}(= 1.8$ T) which is much smaller than the upper critical field. This behavior is usually found in high temperature superconductors where melting of vortices is attributed to thermal fluctuations and very rarely in low T_c superconductors. G_i, which is found to be of the same order as high T_c superconductors, suggests that thermal fluctuations may be playing a role in unpinning of vortices. This is intriguing since most of the low T_c superconductors do not show vortex unpinning due to thermal fluctuations. This seems to be the case here also, since estimation of critical fields was quite straightforward with no significant broadening of thermodynamic measurements with the magnetic field, indicating an unconventional vortex state. Some theoretical and experimental work also suggested that noncentrosymmetric superconductors have an unconventional vortex state [63–66]. Hence, a detailed study on the vortex dynamics of the good quality single crystal of Re_6Hf is needed to interpret these transverse results.

IV. CONCLUSION

A single phase polycrystalline sample of Re_6Hf was prepared by arc-melting technique, which crystallizes into cubic, noncentrosymmetric α-*Mn* (217) structure with lattice cell parameter $a = 9.6850(3)$ Å. Transport, magnetization, and thermodynamic measurements reveal that Re_6Hf is a weakly correlated, type-II superconductor with the bulk transition temperature at $T_c \approx 5.96$ K. Above transition temperature T_c, resistivity measurement showed the poor metallic behavior whereas magnetization measurement showed weak paramagnetism. The computed value of the upper critical field $H_{c2}(0)(\approx 12.2$ T) is close to the Pauli limiting field, hence further investigations need to be done to explore the

TABLE II. Normal and superconducting properties of Re_6Hf.

Parameters	unit	Re_6Hf	Re_6Zr [42]
T_c	K	5.96	6.7
ρ_0	$\mu\Omega$ cm	106.12	137
A	$\mu\Omega$ cm K^{-2}	0.0028	0.008
$H_{c1}(0)$	mT	5.6	8
$H_{c2}(0)$	T	12.2	11.6
$H_{c2}^{\text{orbital}}(0)$	T	9.8	10.65
$H_{c2}^{P}(0)$	T	11.1	12.2
ξ_{GL}	Å	52	53.3
λ_{GL}	Å	3538	3696
k_{GL}		68.0	69.3
γ_n	mJ mol^{-1} K^{-2}	27.2	27.4
θ_D	K	364	330
$\Delta C_{el}/\gamma_n T_c$		1.53	1.62

possible mixture of singlet and triplet pairing states. Low temperature specific heat measurement indicates that Re_6Hf is a moderately coupled superconductor and it was further confirmed by the field dependence of Sommerfeld coefficient $\gamma(H)$ where it varies linearly with H suggesting that electronic states near the Fermi surface are fully gapped. A similar type of behavior was observed in Re_6Zr in its initial measurements. Experimentally estimated values of all the parameters for our sample and Re_6Zr are summarized in Table II. From Table II it is very clear that Re_6Zr and Re_6Hf parameters are almost the same despite Re_6Hf having much stronger spin-orbital coupling strength compared to Re_6Zr. These results suggest that along with spin-orbital coupling strength some other mechanism/phenomena is playing a role in determining the strength of spin-singlet and spin-triplet pairing channel. In order to fully understand the role of spin-orbital coupling, further experimental work on high-quality single crystals is required.

Note. Recently, we became aware that superconductivity was reported on the same compound by another group [67].

ACKNOWLEDGMENTS

We are grateful for valuable discussions with P. Biswas. R.P.S. acknowledges Science and Engineering Research Board, Government of India for the Ramanujan Fellowship through Grant No. SR/S2/RJN-83/2012.

[1] J. Bardeen, L. N. Cooper, and J. R. Schrieffer, Phys. Rev. **108**, 1175 (1957).
[2] P. W. Anderson, J. Phys. Chem. Solids **11**, 26 (1959).
[3] P. W. Anderson, Phys. Rev. B **30**, 4000 (1984).
[4] E. Bauer, G. Hilscher, H. Michor, Ch. Paul, E. W. Scheidt, A. Gribanov, Yu. Seropegin, H. Noël, M. Sigrist, and P. Rogl, Phys. Rev. Lett. **92**, 027003 (2004).
[5] V. M. Edel'shtein, Sov. Phys. JETP **68**, 1244 (1989).
[6] L. P. Gor'kov and E. I. Rashba, Phys. Rev. Lett. **87**, 037004 (2001).
[7] K. V. Samokhin, E. S. Zijlstra, and S. K. Bose, Phys. Rev. B **69**, 094514 (2004).
[8] P. A. Frigeri, D. F. Agterberg, A. Koga, and M. Sigrist, Phys. Rev. Lett. **92**, 097001 (2004).
[9] S. Fujimoto, J. Phys. Soc. Jpn. **76**, 051008 (2007).
[10] M. Nishiyama and Y. Inada, and Guo-qing Zheng, Phys. Rev. Lett. **98**, 047002 (2007).
[11] E. Bauer and M. Sigrist, *Non-centrosymmetric Superconductor: Introduction and Overview* (Springer-Verlag, Heidelberg, 2012).
[12] N. Kimura, K. Ito, K. Saitoh, Y. Umeda, H. Aoki, and T. Terashima, Phys. Rev. Lett. **95**, 247004 (2005).
[13] N. Kimura, K. Ito, H. Aoki, S. Uji, and T. Terashima, Phys. Rev. Lett. **98**, 197001 (2007).
[14] I. Sugitani, Y. Okuda, H. Shishido, T. Yamada, A. Thamizhavel, E. Yamamoto, T. D. Matsuda, Y. Haga, T. Takeuchi, R. Settai, and Y. Ōnuki, J. Phys. Soc. Jpn. **75**, 043703 (2006).
[15] R. Settai, Y. Miyauchi, T. Takeuchi, F. Lévy, I. Sheikin, and Y. Ōnuki, J. Phys. Soc. Jpn. **77**, 073705 (2008).
[16] R. Settai, I. Sugitani, Y. Okuda, A. Thamizhavel, M. Nakashima, Y. Ōnuki, and H. Harima, J. Magn. Mater. **310**, 844 (2007).
[17] T. Akazawa, H. Hidaka, H. Kotegawa, T. C. Kobayashi, T. Fujiwara, E. Yamamoto, Y. Haga, R. Settai, and Y. Ōnuki, J. Phys. Soc. Jpn. **73**, 3129 (2004).
[18] P. Badica, T. Kondo, and K. Togano, J. Phys. Soc. Jpn. **74**, 1014 (2005).
[19] K. Togano, P. Badica, Y. Nakamori, S. Orimo, H. Takeya, and K. Hirata, Phys. Rev. Lett. **93**, 247004 (2004).
[20] P. Badica, T. Kondo, T. Kudo, Y. Nakamori, S. Orimo, and K. Togano, Appl. Phys. Lett. **85**, 4433 (2004).
[21] H. Takeya, K. Hirata, K. Yamaura, K. Togano, M. ElMassalami, R. Rapp, F. A. Chaves, and B. Ouladdiaf, Phys. Rev. B **72**, 104506 (2005).
[22] H. Q. Yuan, D. F. Agterberg, N. Hayashi, P. Badica, D. Vandervelde, K. Togano, and M. Sigrist, and M. B. Salamon, Phys. Rev. Lett. **97**, 017006 (2006).
[23] J. Chen, L. Jiao, J. L. Zhang, Y. Chen, L. Yang, M. Nicklas, F. Steglich, and H. Q. Yuan, New J. Phys. **15**, 053005 (2013).
[24] V. K. Pecharsky, L. L. Miller, and K. A. Gschneidner, Phys. Rev. B **58**, 497 (1998).
[25] J. Chen, M. B. Salamon, S. Akutagawa, J. Akimitsu, J. Singleton, J. L. Zhang, and L. Jiao, and H. Q. Yuan, Phys. Rev. B **83**, 144529 (2011).
[26] S. Kuroiwa, Y. Saura, J. Akimitsu, M. Hiraishi, M. Miyazaki, K. H. Satoh, S. Takeshita, and R. Kadono, Phys. Rev. Lett. **100**, 097002 (2008).
[27] P. K. Biswas, M. R. Lees, A. D. Hillier, R. I. Smith, W. G. Marshall, and D. McK. Paul, Phys. Rev. B **84**, 184529 (2011).
[28] T. Klimczuk, F. Ronning, V. Sidorov, R. J. Cava, and J. D. Thompson, Phys. Rev. Lett. **99**, 257004 (2007).
[29] Y. Qi, J. Guo, H. Lei, Z. Xiao, T. Kamiya, and H. Hosono, Phys. Rev. B **89**, 024517 (2014).
[30] E. Bauer, G. Rogl, X.-Q. Chen, R. T. Khan, H. Michor, G. Hilscher, E. Royanian, K. Kumagai, D. Z. Li, Y. Y. Li, R. Podloucky, and P. Rogl, Phys. Rev. B **82**, 064511 (2010).
[31] A. B. Karki, Y. M. Xiong, I. Vekhter, D. Browne, P. W. Adams, D. P. Young, K. R. Thomas, J. Y. Chan, H. Kim, and R. Prozorov, Phys. Rev. B **82**, 064512 (2010).
[32] T. Shibayama, M. Nohara, H. Aruga Katori, Y. Okamoto, Z. Hiroi, and H. Takagi, J. Phys. Soc. Jpn. **76**, 073708 (2007).
[33] K. Wakui, S. Akutagawa, N. Kase, K. Kawashima, T. Muranaka, Y. Iwahori, J. Abe, and J. Akimitsu, J. Phys. Soc. Jpn. **78**, 034710 (2009).
[34] N. Kase and J. Akimitsu, J. Phys. Soc. Jpn. **78**, 044710 (2009).
[35] L. Fang, H. Yang, X. Zhu, G. Mu, Z. Sheng Wang, L. Shan, C. Ren, and H.-Hu Wen, Phys. Rev. B **79**, 144509 (2009).
[36] R. P. Singh, N. A. Parzyk, M. R. Lees, D. M. Paul, and G. Balakrishnan, J. Cryst. Growth **395**, 22 (2014).
[37] A. B. Karki, Y. M. Xiong, N. Haldolaarachchige, S. Stadler, I. Vekhter, P. W. Adams, D. P. Young, W. A. Phelan, and J. Y. Chan, Phys. Rev. B **83**, 144525 (2011).
[38] C. S. Lue, T. H. Su, H. F. Liu, and B. L. Young, Phys. Rev. B **84**, 052509 (2011).

[39] J. Chen, L. Jiao, J. L. Zhang, Y. Chen, L. Yang, M. Nicklas, F. Steglich, and H. Q. Yuan, Phys. Rev. B **88**, 144510 (2013).
[40] J. A. T. Barker, D. Singh, A. Thamizhavel, A. D. Hillier, M. R. Lees, G. Balakrishnan, D. McK. Paul, and R. P. Singh, Phys. Rev. Lett. **115**, 267001 (2015).
[41] R. P. Singh, A. D. Hillier, B. Mazidian, J. Quintanilla, J. F. Annett, D. M. Paul, G. Balakrishnan, and M. R. Lees, Phys. Rev. Lett. **112**, 107002 (2014).
[42] A. M. Khan, arXiv:1603.07297.
[43] A. D. Hillier, J. Quintanilla, and R. Cywinski, Phys. Rev. Lett. **102**, 117007 (2009).
[44] H. Takeya, M. ElMassalami, and S. Kasahara, and K. Hirata, Phys. Rev. B **76**, 104506 (2007).
[45] C. S. Lue, H. F. Liu, C. N. Kuo, P. S. Shih, J-Y. Lin, Y. K. Kuo, M. W. Chu, T-L Hung, and Y. Y. Chen, Superconduct. Sci. Tech. **26**, 055011 (2013).
[46] F. von Rohr, H. Luo, N. Ni, M. Wörle, and R. J. Cava, Phys. Rev. B **89**, 224504 (2014).
[47] W. L. McMillan, Phys. Rev. **167**, 331 (1968).
[48] M. Isobe, A. Masao, and N. Shirakawa, Phys. Rev. B **93**, 054519 (2016).
[49] C. Caroli, P. G. de Gennes, and J. Matricon, Phys. Lett. **9**, 307 (1964).
[50] P. G. de Gennes, *Superconductivity of Metals and Alloys* (W. A. Benjamin, New York, 1966).
[51] G. E. Volovik, JETP Lett. **58**, 469 (1993).
[52] K. Kadowaki and S. B. Woods, Solid State Commun. **58**, 507 (1986).
[53] R. Jin, J. He, S. McCall, C. S. Alexander, F. Drymiotis, and D. Mandrus, Phys. Rev. B **64**, 180503 (2001).
[54] A. C. Jacko, J. O. Fjaerestad, and B. J. Powell, Nat. Phys. **5**, 422 (2009).
[55] M. Tinkham, *Introduction to Superconductivity*, 2nd ed. (McGraw-Hill, New York, 1996).
[56] E. Helfand and N. R. Werthamer, Phys. Rev. **147**, 288 (1966).
[57] N. R. Werthamer, E. Helfand, and P. C. Hohenberg, Phys. Rev. **147**, 295 (1966).
[58] B. S. Chandrasekhar, Appl. Phys. Lett. **1**, 7 (1962).
[59] A. M. Clogston, Phys. Rev. Lett. **9**, 266 (1962).
[60] K. Maki, Phys. Rev. **148**, 362 (1966).
[61] O. Prakash, A. Thamizhavel, and S. Ramakrishnan, Supercond. Sci. Technol. **28**, 15012 (2015).
[62] G. Blatter, M. V. Feigel'man, V. B. Geshkenbein, and A. I. Larkin, and V. M. Vinokur, Rev. Mod. Phys. **66**, 1125 (1994).
[63] M. Sigrist and D. F. Agterberg, Prog. Theor. Phys. **102**, 965 (1999).
[64] E. Dumont and A. C. Mota, Phys. Rev. B **65**, 144519 (2002).
[65] C. F. Miclea, A. C. Mota, M. Sigrist, F. Steglich, T. A. Sayles, B. J. Taylor, C. A. McElroy, and M. B. Maple, Phys. Rev. B **80**, 132502 (2009).
[66] C. F. Miclea, A. C. Mota, M. Nicklas, R. Cardoso, F. Steglich, M. Sigrist, A. Prokofiev, and E. Bauer, Phys. Rev. B **81**, 014527 (2010).
[67] B. Chen, Y. Guo, H. Wang, Q. Su, Q. Mao, J. Du, Y. Zhou, J. Yang, and M. Fang, Phys. Rev. B **94**, 024518 (2016).